The Ciência & Engenharia - Science & Engineering Journal
ISSN: 0103-944X
Volume 11 Issue 1, 2023
pp: 2350-2363

Induction Motor Thermal Model for Optimal Air-Cooling Strategies and Monitoring

[1]Željko Špoljarić, [1]Željko Hederić, [1]Vedrana Jerković Štil, [1]Krešimir Miklošević
[1] Faculty of Electrical Engineering, Computer Science and Information Technology Osijek, Kneza Trpimira 2b, HR-31000 Osijek, Croatia
[1]zeljko.spoljaric@ferit.hr,[2]zeljko.hederic@ferit.hr, [3]vedrana.jerkovic@ferit.hr, [4]kresimir.miklosevic@ferit.hr

Abstract— Optimal air-cooling strategies can lead to significant energy savings to increase the energy efficiency. To analyze a thermodynamic behavior of an automated industrial plant all parts of plant should be taken into account, which is a very complex issue. This paper proves that for passive cooling of induction motor the simple model which only takes into account the stator thermodynamic behavior is enough. One – dimensional thermal map of tested induction motor is constructed. Totally enclosed fan cooled induction motor thermodynamic model with analogous electrical scheme and mathematical equations is given. Simulation results are compared to measurements and they show that the proposed thermodynamic stator model describes the passive stator cooling process well**.**

Index Terms— induction motor, thermal map, thermodynamic model, energy efficienc

Introduction

Today, air conditioning has become a necessity in building, dwellings and industrial processes and has become the largest energy end use both in the residential and non-residential sector [1].

This being the case, the optimal air-cooling strategies can lead to significant energy savings and to the increase of energy efficiency. To design an optimal operation of air conditioning in the automated industrial plant, the thermodynamic behavior of all parts of plant should be taken into account, which is a very complex issue. In this paper we prove that for passive cooling of induction motor the simple model which only takes into account the stator thermodynamic behavior is enough. The thermodynamic model of a total enclosed fan cooled induction motor (TEFC) is given in [2].

In [3] authors presented the development and validation of a time-dependent lumped-parameter thermal model of an induction motor that can be used to identify potential design enhancements to minimize the internal temperature during operation. The model was validated by comparison of calculated and experimental data of motor temperature during motor operation (loaded stage). In order to get a reasonable prediction of the operating motor temperature, the knowledge of cooling air speed is needed.

In [4] the authors made a sensitivity analysis of model parameters necessary for induction motor thermal model. The comparison was done for five motors and two different methods. The analysis has point out that the speed of cooling air changes along the motor axial length

The Ciência & Engenharia - Science & Engineering Journal
ISSN: 0103-944X
Volume 11 Issue 1, 2023
pp: 2350-2363

and is maximum at the cowling outlet. These results should be taken into account when calculating the forced convection heat transfer coefficient, which is then combined with the natural convection heat transfer coefficient. Also for more accurate motor thermal model, knowledge of geometrical and material properties of analyzed motor a crucial for accurate prediction of thermal performance during motor operation like explained in [5]. In this paper the temperature measurements

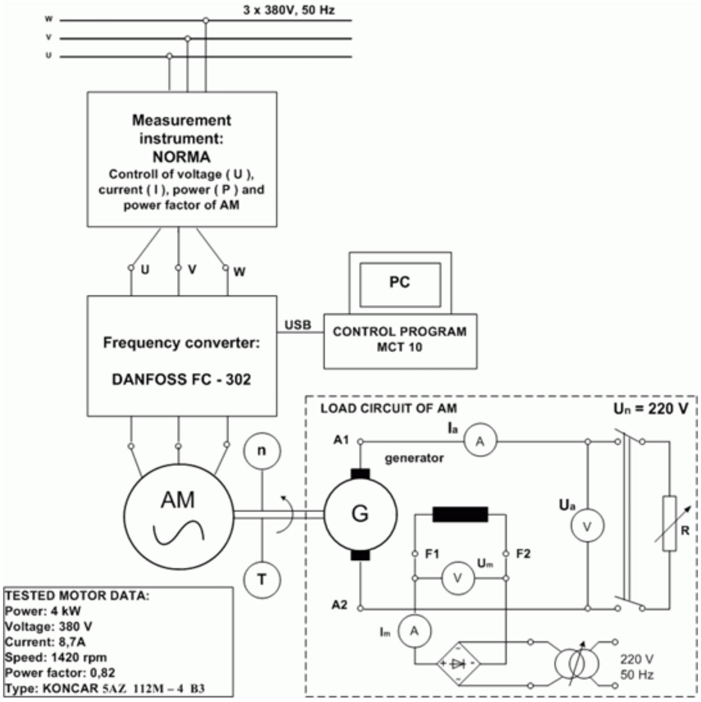

Figure 1. Block scheme of induction motor heating process.

were taken and analyzed during the motor passive cooling process. In the beginning the 4kW totally enclosed fan cooled motor was running for a certain period of time at nominal operation point. Block scheme for induction motor heating process connected with DC generator as load and tested motor data is shown in Fig.1. and also given in [6]. After that period, the motor is disconnected from the power supply and stopped and the passive cooling process takes a place. This way the ventilation effect and cooling air speed changes can be neglected.

Measurement Analysis

The motor heating measurements were taken from starting temperature of 20 °C and measured winding resistance in cool state of 3,375 Ω. After the heating process the temperature measurements were taken on the three different places: on the housing front section (ϑ_1), on the active housing section (ϑ_2) and on the housing rear section (ϑ_3) as shown in Fig. 2a. Measurements were taken by using infrared thermometer (IR) FLUKE 568 as shown in Fig. 2b. The winding temperature (ϑ_w) is estimated according to (1) by using measured DC current and voltage values during the motor cooling. Measured and estimated values are given in the Table I.

The Ciência & Engenharia - Science & Engineering Journal
ISSN: 0103-944X
Volume 11 Issue 1, 2023
pp: 2350-2363

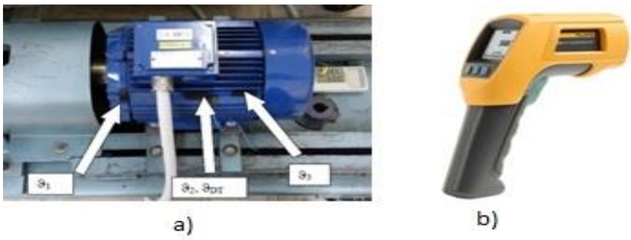

Figure 2. IR temperature measurements on induction motor housing (a) with FLUKE 568 IR thermometer (b).

$$\vartheta_w = \vartheta_{w0} + \frac{1}{\alpha_{Cu}}\left(\frac{R_w}{R_{w0}} - 1\right) \qquad (1)$$

In (1) the R_w represents the calculated winding resistance, R_{w0} = 3,375 Ω represents the winding resistance at the ambient temperature ϑ_{w0} = 20 °C, α_{Cu} represents the thermal conductivity of copper, the material of which the motor winding is made (α_{Cu} = 0,0039 K^{-1}).
The temperatures measured during motor cooling are presented in Fig. 2. In Fig. 3 four curves are showed. Three curves represent the housing temperatures on three different motor sections (housing 1 - ϑ_1, housing 2 - ϑ_2 and housing 3 – ϑ_3) and one curve (winding) presents the temperature of motor winding gained by (1). In the beginning of a motor cooling process, the winding temperature drops rapidly from its initial value of 50.1 °C to temperature slightly bigger than those recorded on the motor housing. On the other hand, after the motor is disconnected and stopped, in the beginning of motor cooling process the temperatures on the motor housing still continue to grow and reach their maximal value after 3

Table I. Measured and estimated motor temperatures.

Time (min)	ϑ_1 (°C)	ϑ_2 (°C)	ϑ_3 (°C)	R_w (Ω)	ϑ_w (°C)
0	39.8	40.7	39.0	3.817	50.1
1	39.8	41.0	39.8	3.733	43.8
3	39.8	41.0	40.2	3.715	42.5
7	39.3	40.6	40.0	3.704	41.7
12	38.9	40.0	39.8	3.696	41.1
17	37.9	39.6	39.5	3.685	40.2
22	37.5	38.6	38.5	3.674	37.4
27	37.1	38.1	38.0	3.667	38.9
37	35.7	36.9	36.6	3.651	37.7
47	34.3	35.4	35.1	3.624	35.7
57	33.5	34.5	34.3	3.615	35.0
90	29.6	30.3	30.2	3.557	30.6
120	27.8	28.0	28.0	3.532	28.7
180	25.4	25.5	25.0	3.493	25.8
230	24.1	24.1	24.0	3.480	24.8

The Ciência & Engenharia - Science & Engineering Journal
ISSN: 0103-944X
Volume 11 Issue 1, 2023
pp: 2350-2363

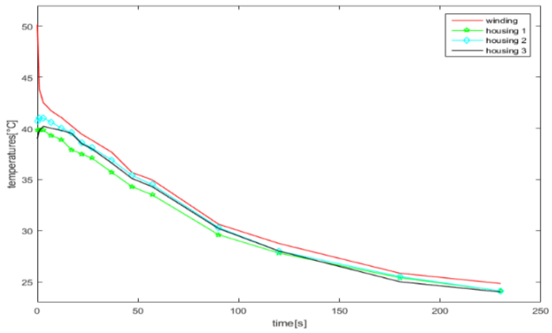

Figure 3. The estimated winding temperature and the measured housing temperatures during the motor cooling.

minutes. After that period all temperatures drop slowly during the time. The measurements show that the highest housing temperature is reached in the active housing section. These results correspond to results reported in [7] where authors based on infrared images taken from hottest motor part on motor surface detect short circuit faults in the stator windings. Correlations between fault severity with temperature amount on motor surface are made. In addition, the measured housing temperatures provide the possibility of constructing the one-dimensional motor thermal map in the time as presented in Fig. 4.

It is visible from Fig. 4 that temperature is highest in starting of cooling process and then it drops to ambient temperature after some period of time. Also, temperature is highest in induction motor middle section (housing 2 - ϑ_2).

II. Induction Motor Stator Thermal Model

The recorded cooling process is suitable for TEFC motor stator model testing. The motor stator consists of stator windings, stator iron core made of laminated steel and motor silumin housing. All of three mentioned components show properties of thermal resistance and thermal capacitance so the motor stator thermal model can be represented with the equivalent electrical scheme, as shown in Fig.5.

The regular structure and the symmetry of the machine makes it possible to divide the machine into elements that are

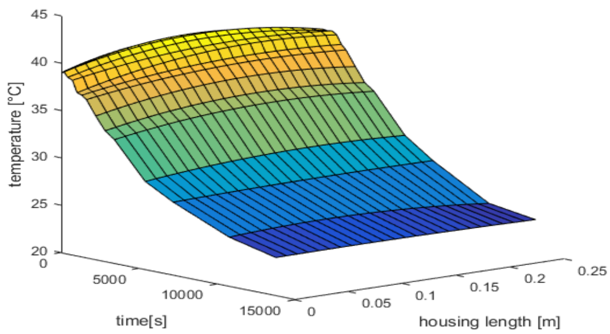

Figure 4. One – dimensional motor thermal map in the time.

The Ciência & Engenharia - Science & Engineering Journal
ISSN: 0103-944X
Volume 11 Issue 1, 2023
pp: 2350-2363

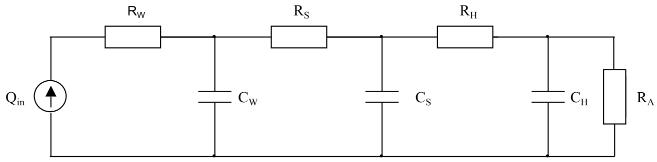

Figure 5. Equivalent electrical scheme of induction motor thermal system.

concentric around the shaft. Combing thermal model and electromagnetic motor model gives possibility for electro-magneto-thermal analysis [8].

The modelled heat source corresponds to the stator winding losses, i.e. $Q_{in} = P_{Cu,S} = 3i_sR_w$, where Q_{in} is input heat flow, $P_{Cu,S}$ is stator winding losses, i_s represents the phase stator current and R_w is stator winding resistance. The heat is transferred through the stator components by conduction to the housing surface from which is dissipated by convection in the surrounding air.

The stator winding and housing temperatures ϑ_W and ϑ_H are equivalent to corresponding voltages. The currents occurring in the equivalent electrical circuit correspond to the stator heat flows. The R_W, R_S and R_H represent the thermal resistances of stator winding, stator core and stator housing, respectively. The R_A represents the thermal resistance for a convective heat transfer to the air.

From equivalent electrical scheme presented in Fig.5. the transfer function $H_w(s)$ which describes the winding temperature dynamics ϑ_W in respect to input heat flow Q_{in} is gained:

$$H_w(s) = \frac{\vartheta_w(s)}{Q_{in}(s)} = \frac{B_w(s)}{A_w(s)} \qquad (2)$$

where the polynom $B_w(s)$ equals:

$$B_w(s) = R_W A s^3 + \{R_W[T_{SW}B + T_{AH}C] + R_W D\}s^2 + \\ +[R_W E + R_S.B + R_H\,T_{AH}]s + R_W + R_S + R_H + R_A \qquad (3)$$

and where:

$$A = T_{SW}T_{HS}T_{AH} \qquad (4)$$

$$B = T_{AS} + T_{HS} + T_{AH} \qquad (5)$$

$$C = T_{HW}T_{HS} \qquad (6)$$

$$D = T_{HS}T_{AH} \qquad (7)$$

$$E = T_{AW} + T_{HW} + T_{SW} + T_{AS} + T_{HS} + T_{AH} \qquad (8)$$

Polynom $A_w(s)$ equals:

$$A_w(s) = As^3 + [T_{SW}B + T_{AH}C]s^2 + Es + 1 \qquad (9)$$

The time constants used in winding transfer function $H_w(s)$ are equal as follows: $T_{SW} = R_sC_W$, $T_{HS} = R_HC_S$, $T_{AH} = R_AC_H$, $T_{AS} = R_AC_S$, $T_{HW} = R_HC_W$ and $T_{AW} = R_AC_W$.

The transfer function that describes the dynamics of housing temperature ϑ_H with respect to the input heat flow can be written as:

$$H_H(s) = \frac{\vartheta_H(s)}{Q_H(s)} \cdot \frac{Q_H(s)}{Q_{in}(s)} \qquad (10)$$

Table II. Tested motor stator material properties and dimensions.

	Stator winding (insulated copper wire)	**Stator core** (laminated steel)	**Stator housing** (pressure die cast silumin)
Thermal conductivity (W/mK)	400	28	163
Heat capacity (J/kgK)	390	490	900
Mass density (kg/m^3)	8900	7650	2700
Length (m)	0,140	0,140	0,310
Area (m^2)	3,3 $\cdot 10^{-3}$	14,3 $\cdot 10^{-3}$	2,7$\cdot 10^{-3}$

where the variable Q_H represents the housing heat flow, which can be presented in the following manner by using equivalent scheme (Fig. 5):

$$Q_H(s) = H_1(s)Q_{in}(s) + H_2(s)\vartheta_w(s) = H_1(s)Q_{in}(s) + H_2(s)H_w(s)Q_{in}(s) = \big(H_1(s) + H_2(s)H_w(s)\big)Q_{in}(s) \qquad (11)$$

The transfer function describing the housing heat flow dynamics with respect to the input heat flow is then:

$$\frac{Q_H(s)}{Q_{in}(s)} = H_1(s) + H_2(s)H_w(s) \qquad (12)$$

where the transfer functions $H_1(s)$ and $H_2(s)$ equal:

$$H_1(s) = \frac{T_W T_{AH} s^2 + (T_W + T_{AH})s + 1}{T_{HS} T_{AH} s^2 + (T_{HS} + T_{AS} + T_{AH})s + 1} \qquad (13)$$

$$H_2(s) = \frac{C_W T_{AH} s^2 + C_W s + 1}{T_{HS} T_{AH} s^2 + (T_{HS} + T_{AS} + T_{AH})s + 1} \qquad (14)$$

Where the winding time constant T_W equals:

$$T_W = R_W C_W \qquad (15)$$

Finally, the transfer function that gives the housing temperature dynamics with respect to the housing heat flow is:

$$H_H(s) = \frac{\vartheta_H(s)}{Q_H(s)} = \frac{R_A}{T_{AH} s + 1} \qquad (16)$$

The equations (3), (10), (12), (13) and (14) represents a thermodynamic model of an TEFC motor stator. This model is neglecting the rotor, air gap and ventilation thermal influence on thermal conditions in the motor stator and is therefore rather simple and suitable for research of passive cooling process. It requires the knowledge of stator materials and dimensions.
The gained thermodynamic stator model is used for

Table III. Tested motor stator parameters.

	Stator winding (insulated copper wire)	**Stator core** (laminated steel)	**Stator housing** (pressure die cast silumin)
Thermal resistance (K/W)	$4{,}138 \cdot 10^{-4}$	$140 \cdot 10^{-4}$	$1{,}8 \cdot 10^{-4}$
Heat capacity (J/kgK)	$1{,}625 \cdot 10^{3}$	$5{,}765 \cdot 10^{3}$	$4{,}858 \cdot 10^{3}$

simulation of tested TEFC motor in Matlab 2015 software package. The material properties of stator winding, core and housing, as well as the stator dimensions of the tested motor from manufacturer are given in the Table II. The calculated model parameters are given in the Table III. The convective heat transfer coefficient is 8 W/m^{2}K. Simulation results are compared to measurements.

The Ciência & Engenharia - Science & Engineering Journal
ISSN: 0103-944X
Volume 11 Issue 1, 2023
pp: 2350-2363

Simulation Results

As there is no rotor or ventilation effect taken into account in the model, the simulated time of stator heating must be considerably shorter than the time needed to heat the real motor stator to the same temperatures, which are the initial conditions for the passive cooling process.

The simulation results are compared to the measurements of the winding temperature and the active housing section temperature. The simulation results are shown in the following figures. Fig. 6. shows that the proposed thermodynamic stator model describes the passive stator cooling process well and that the thermal influence of rotor and air gap during that process can be neglected.

In Fig. 7 it can be seen that the measured and simulated stator winding temperatures (Fig.7a) during the motor cooling are matching almost perfectly. In Fig. 7b there is comparison between measured and simulated housing temperature. The differences (Fig. 7c) in measured and simulated stator winding temperature arise from the measurement uncertainty.

On the other hand, the starting measured housing temperature is slightly lower than the simulated one. This difference arises from the simplification in model.

Namely, the simplified model cannot be brought by applying the step function at the input at the exact same conditions as one found in the real motor, because this model does not describe the heating of motor stator well. For the heating process the another model, which takes into account the other motor parts, should be used.

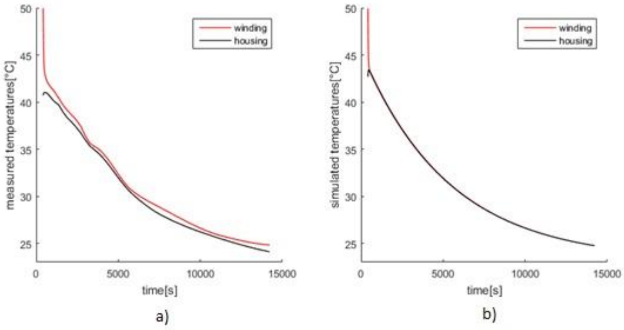

Figure 6. The measured (a) and simulated (b) winding and housing temperatures during the passive cooling process.

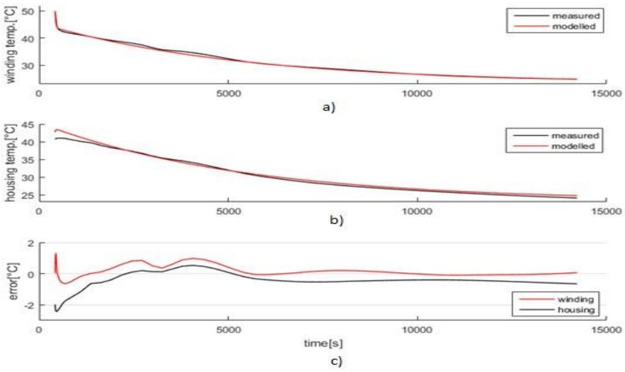

Figure 7. The comparison of measured and simulated winding (a), active housing (b)section temperatures and error between sections (c).

The Ciência & Engenharia - Science & Engineering Journal
ISSN: 0103-944X
Volume 11 Issue 1, 2023
pp: 2350-2363

IV. Thermal Monitoring System

The embedded condition monitoring of rotating electrical machines such as motors and generators in purpose of failure prediction and failure recognition in early stage when a crucial damage to the monitoring machine did not yet occur presents a challenging task. Regarding rotating machines monitoring, as monitoring of induction motors, diagnostic applications are focused on detection of bearing and insulation failures with using thermal, vibration, acoustic, magnetic and partial discharge sensors [9].

Mostly this monitoring systems are embedded in one system. In this paper the accent is given on thermal diagnostic system. Possibility to measure the temperatures in in few points on electrical machine housing gives opportunity to create a motor thermal image. The problem that may occur is recognition of hottest point or Hot-spot measurement [10, 11]. Using a thermal image with hot-spot temperatures of induction machine could be used for motor monitoring and protection as presented in [12-14].

In this way by combining temperature measurements by using data acquisition system (DAQ) in key points (stator core, windings) with TEFC motor model a thermal monitoring system can be constructed (Fig. 8).

Thermal monitoring system of induction motor consists of tested induction motor, data acquisition system (DAQ), thermocouple, PC, software NI LabVIEW for measurements, and thermal motor model in Matlab.

NI (National Instruments) myDAQ is used for data acquisition of induction motor housing temperature measurements (Fig. 9).

NI my DAQ is multifunction device which combines all laboratory instruments necessary for measurement and programing via PC. Combined with software NI LabVIEW (Laboratory Virtual Instrument Engineering Workbench) as explained in [15] and Multisim program for device control it provides a real-time continuous temperature measurement of induction motor housing.

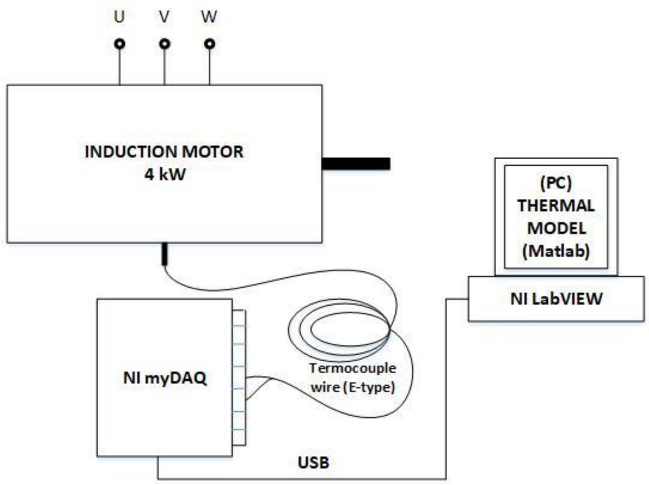

Figure 8. Thermal monitoring system of induction motor.

NI myDAQ consists of: two differential analogous inputs (16 bit, 200 kS/s, ±10 V, ±2 V, DC pair) which are used for oscilloscope, dynamic signal analyzer and Bode analyzer, two

The Ciência & Engenharia - Science & Engineering Journal
ISSN: 0103-944X
Volume 11 Issue 1, 2023
pp: 2350-2363

analogous out (16 bit, 200 kS/s, ±10 V, ±2 V, DC pair) for function generator, generator of wave forms and Bode analyzer, 8 digital inputs/outputs (3,3 V, TTL), DC source (5 V, +15 V, -15 V) up to 500 mW. digital multimeter (DMM), one stereo audio input (±2 V, AC – paired), one digital counter (320bit, base clock 100 MHz) and USB port.

Programing in LabVIEW is based on graphical programing in program language "G" which is adapted for communication with different hardware and measurement equipment like myDAQ card.

Configuration and programing takes place in two different panels: Block Diagram (Fig. 10) and Front Panel (Fig. 11). Programing is done by using three different panels. For programing in Block Diagram where core program is made, a palette Functions is used. For programing in Front Panel where measurement results can be seen and analyzed a palette Controls is used. Palette Tools is used for both program windows. Before temperature measurements a Channels for measurements with myDAQ should be adjusted by using DAQ Assistant tool and card connection diagram as showed in Fig. 12.

Figure 9. NI myDAQ used for temperature measurements.

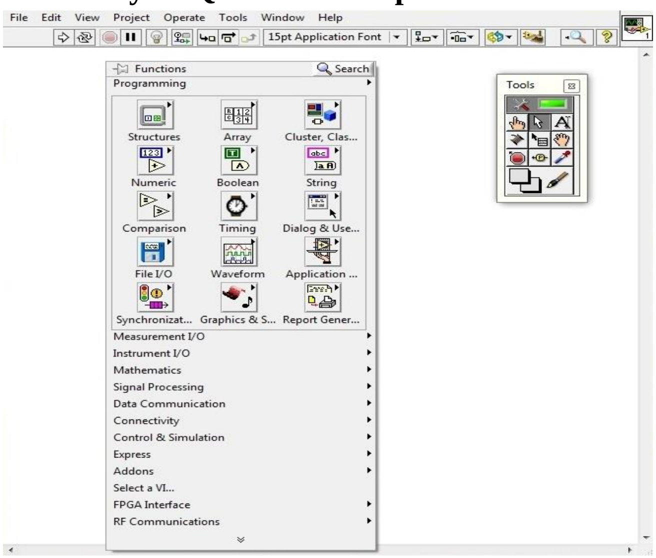

Figure 10. Block Diagram panel and palette Control for programing in LabVIEW.

The Ciência & Engenharia - Science & Engineering Journal
ISSN: 0103-944X
Volume 11 Issue 1, 2023
pp: 2350-2363

Communication between myDAQ measurement card and program LabVIEW is done via USB. Temperature measurements are done by using thermocouple wire type E (material for positive connection (+) Ni-Cr, material for negative connection (-) Cu-Ni) with Seebeck coefficient equals 61 μV/°C. Seebeck coefficient is defined for every thermocouple type and its presents a measure of the magnitude of induced thermoelectric voltage in response to a temperature difference across that material. This is known as Seebeck effect and given in [16]. The temperature range of E type thermocouple is from -270 °C to 1000 °C. Thermocouple positive line should be connected on positive connector (+0) of myDAQ and thermocouple negative line should be connected on negative connector (-0) of myDAQ as also defined in Fig. 12.

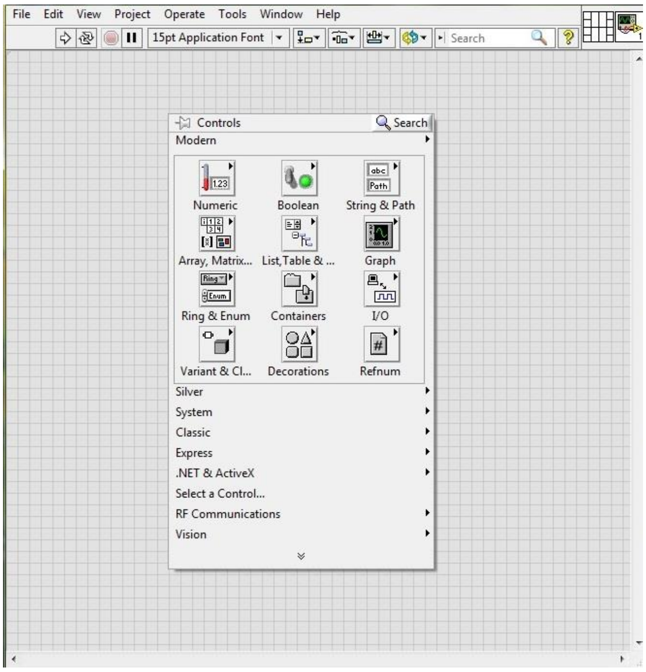

Figure 11. Front panel and palette Functions for programing in LabVIEW.

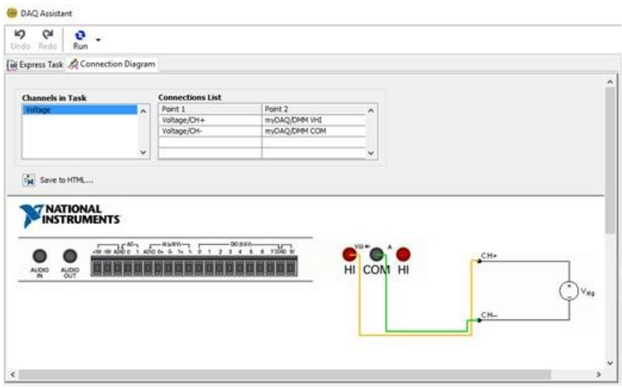

Figure 12. Configuration of measurement Channels.

It is important to mention that for correct measurement of induction motor housing temperature it is important to connect cold junction connection (CJC) where the thermocouple wire is

The Ciência & Engenharia - Science & Engineering Journal
ISSN: 0103-944X
Volume 11 Issue 1, 2023
pp: 2350-2363

connected to myDAQ card. Cold junction sensor minimizes temperature gradient between the cold junction sensor and thermocouple wire connection.

Fig. 13 presents the monitoring of induction motor housing temperature. These measurements which are done by myDAQ card and LabVIEW program are input data in motor thermal model which is made in Matlab 2015 and provides a thermal monitoring system of induction motor.

Conclusion

Diagnostic and monitoring of rotating electrical machines and industrial drive systems presents a complex and challenging work. Embedded systems for monitoring and control are mostly used for monitoring and diagnostic of higher power motors and generators because of the price of such systems and where it is not possible to replace a damaged machine in short time. One of systems for monitoring, control and failure prevention (prediction) is a thermal monitoring system like one used for thermal monitoring of induction motor in this paper.

Before development of thermal monitoring system, it is necessary to measure motor heating and cooling characteristic as well as knowing the motor material properties and dimensions for proper adjustment of created motor thermal model. Presented motor thermal model characteristics is its simplicity and it is based on monitoring stator winding temperatures on motor housing (surface).

The measured and simulated stator winding temperatures

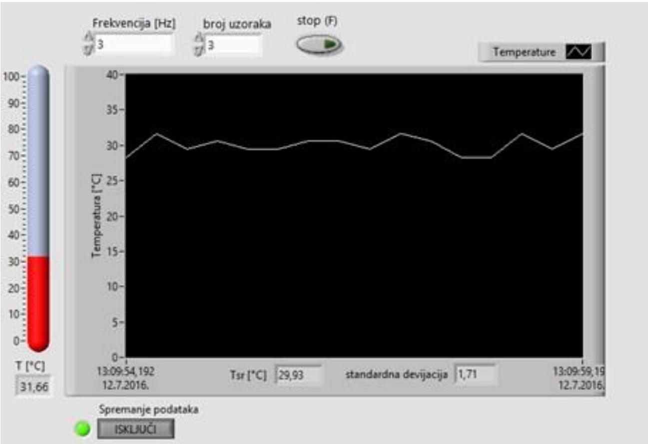

Figure 13. Induction motor temperature measurements and monitoring using NI myDAQ.

during motor cooling process are matching almost perfectly which confirms the model accuracy. Also, by knowing the motor thermal map in time it is possible to increase the energy efficiency and reduce the energy consumption that may occur if motor is operating in fault mode.

Further research will include combining the motor thermal monitoring system with system for vibration detection in coupled motor-generator drive systems or coupled motor systems which are used for electrical vehicle or propulsion drive systems used for ship drives.

The Ciência & Engenharia - Science & Engineering Journal
ISSN: 0103-944X
Volume 11 Issue 1, 2023
pp: 2350-2363

References

[1] K.J. Chua, S.K. Chou, W.M. Yang and Y. Yan, "Achieving better energy-efficient air conditioning - A review of technologies and strategies", Applied Energy, vol. 104, pp. 87-1014, 2013.

[2] D. Staton, "Induction motor thermal analysis", Strojarstvo (Mechanical Engineering), vol. 51, no. 6, pp. 623-631, 2009.

[3] T.A. Jankowski, F.C.Preger, D.D. Hill, S.R. O´Bryan, K.K. Sheth, E.B. Brookbank, D.F.A. Hunt, Y.A. Orrego, "Dvelopent and validation of a thermal model for electric induction motors", IEEE Trans. On Industrial Electronics, vol. 57, no. 12, pp. 4043-4054, December 2010.

[4] A. Boglietti, A. Cavagnino and D. A. Staton, "TEFC induction motors thermal models: A parameter sensitivity analysis", IEEE Trans. on Industry Applications, vol. 41, no. 3, May/June 2005.

[5] A. Boglietti, A. Cavagnino and D. A. Staton, "Thermal analysis of TEFC induction motors, 38th IAS Annual Meeting on Conference Record of the Industry Applications Conference, 2003.

[6] K. Miklosevic, Z. Spoljaric and Z. Valter, "Modeling and simulation of induction motor for dynamic behavior testing using specified load", Annals of DAAAM for 2008 & Proceedings of the 19th International DAAAM Symposium, pp.431, 2008.

[7] M. Eftekhari, M. Moallem, S. Sadri and M.F. Hsieh, "A novel indicator of stator winding inter-turn fault in induction motor using infrared thermal imaging", Infrared Physics & Technology, vol. 61, pp. 330-336, 2013.

[8] S. Mezani, N. Takorabet and B. Laporte, "A combined electromagnetic and thermal analysis of induction motors", IEEE Trans. on Magnetics, vol. 41, Issue 5, May 2005.

[9] M. Kande, A.J. Isaksson, R. Thottappillil and N. Taylor, "Rotating electrical machine condition monitoring automation – A Review", MDPI, Machines, vol. 5, no. 24, October 2017.

[10] P.J. Tavner, "Review of condition monitoring of rotating electrical machines", IET Electric Power Applications, vol. 2, no. 4, pp. 215-247, 2008.

[11] P. Tavner, L. Ran, J. Penman and H. Sedding, "Condition monitoring of rotating electrical machines", The Institution of Engineering and Technology, London, United Kingdom, 2008.

[12] Kathole, A. B., Katti, J., Dhabliya, D., Deshpande, V., Rajawat, A. S., Goyal, S. B., . . . Suciu, G. (2022). Energy-aware UAV based on blockchain model using IoE application in 6G network-driven cybertwin. Energies, 15(21) doi:10.3390/en15218304

[13] Keerthi, R. S., Dhabliya, D., Elangovan, P., Borodin, K., Parmar, J., & Patel, S. K. (2021). Tunable high-gain and multiband microstrip antenna based on liquid/copper split-ring resonator superstrates for C/X band communication. Physica B: Condensed Matter, 618 doi:10.1016/j.physb.2021.413203

[14] Kothandaraman, D., Praveena, N., Varadarajkumar, K., Madhav Rao, B., Dhabliya, D., Satla, S., & Abera, W. (2022). Intelligent forecasting of air quality and pollution prediction

using machine learning. Adsorption Science and Technology, 2022 doi:10.1155/2022/5086622

[15] S.E. Zocholl, “Motor analysis and thermal protection”, IEEE Trans. on Power Delivery, PD-5, pp. 1275-80, 1990.

[16] P. Milanfar and J.H. Lang, “Monitoring the thermal condition of permanent-magnet synchronous motors”, IEEE Trans. on Aerospace and Electronic Systems, AES-32, pp. 1421-29, 1996.

[17] P.H. Mellor, D. Roberts and D.R. Turner, “Lumped parameter thermal model for electrical machines of TEFC design, IEE Proceedings Part B, Electric Power Applications, vol. 138, pp. 205-218, 1991.

[18] Z. Valter, “Process measurements”, Faculty of Electrical Engineering Osijek, Grafika d.o.o. Osijek, Osijek, Croatia, April 2008.

[19] S. Blundell, S.J. Blundell and K.M. Blundell, “Concepts in thermal physics”, Oxford University Press, pp. 415, 2010.